Marine Geology 465 (2023) 107166

Contents lists available at ScienceDirect

Marine Geology

journal homepage: www.elsevier.com/locate/margo

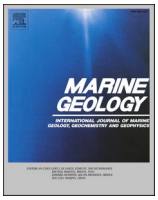

The origin of the Musicians Seamount Province and its inferences for Late Cretaceous Pacific Plate Motion

Andrea Balbas [a,*], Carl Jung [a], Kevin Konrad [b]

[a] Department of Geological Sciences, California State University Long Beach, Long Beach, CA 90840, USA
[b] Department of Geoscience, University of Nevada Las Vegas, Las Vegas, NV 89154, USA

ARTICLE INFO

Editor: Adina Paytan

Keywords:
Musician Seamount Province
$^{40}Ar/^{39}Ar$ geochronology
Volcanic elongated ridges
Plume-Ridge
Absolute Plate Motion
Euterpe Plume

ABSTRACT

Linear chains of seamounts, sourced from mantle plume processes, have the potential to refine plate motion models because the hotspot remains fixed relative to the moving lithospheric plate. However, to define plate motion, consistent seamount age progression and geometry are required. Some seamount chains, such as the Musician Seamount Province (MSP), have complex geometries and age distributions, which complicates calibrating plate motion. The MSP resides northwest of the Hawaiian Islands and is composed of seamounts and volcanic elongated ridges (VERs) that cover ~420,000 km^2 of Pacific seafloor. Here we provide new $^{40}Ar/^{39}Ar$ age determinations for a series of lava flows recovered from the MSP during expedition EX1708 of the National Oceanic and Atmospheric Administration's Ocean Exploration program. The MSP was built by four distinct volcanic processes: (1) age-progressive hotspot volcanism associated with the Euterpe Plume (ca. 98–79 Ma). (2) VER formation from plume-ridge channelization (ca. 97–94 Ma; 86–79 Ma) where the VERs only form when the hotspot is within ~600 km of the ridge. (3) Eocene volcanism driven by extension during the ca. 50 Ma change in Pacific rotation poles (ca. 54–47 Ma). (4) Some near-ridge shear-driven upwelling or diffuse extensional volcanism that preceded the southern MSP lithosphere overriding the plume (ca. 86–84 Ma). By filtering lava flows with only robust statistically concordant $^{40}Ar/^{39}Ar$ age determinations as well as geologic setting, we develop a dataset of samples valuable for constraining Pacific plate motion. A local plate velocity of 42 ± 9 km/Ma for the 98–81 Ma time frame is calculated. Furthermore, the seamount track indicates that large shifts in Pacific rotation pole locations are required prior to 98 Ma and at ca. 81 Ma.

1. Introduction

The age-progressive nature of hotspot tracks has allowed for valuable insights into the past movements of tectonic plates as well as mantle structure and dynamics (Duncan and Clague, 1985; Koppers et al., 2001; Tarduno et al., 2003; Wessel and Kroenke, 2008; Konrad et al., 2018). However, hotspot track geometries become complicated when interacting with proximal spreading centers, often producing unique topographic features (e.g., Martin et al., 2011; Mittal and Richards, 2017; Long et al., 2019; Jiang et al., 2021). Plumes underlying ridges can commonly generate anomalous amounts of melting, sometimes forming a large igneous province or rises (e.g. Shatsky Rise; Nakanishi et al., 1999; Dürkefälden et al., 2021). Alternatively, when a plume resides near a spreading center (e.g. within 1000 km) channels of enriched mantle, with or without melt, can develop between the two upwelling centers, resulting in the production of chains of small volcanos that grow together into volcanic elongated ridges (VERs; e.g. Kopp et al., 2003; Mittal and Richards, 2017). Understanding the drivers for these processes requires direct sampling and analyses of lava flows. Here we focus one complex region of oceanic lithosphere that has been argued to be affected by multiple intraplate volcanic process—the Musician Seamount Province (MSP).

2. Geologic setting

The MSP is a complex region of Pacific lithosphere comprised of three or more distinct features and trends (Rea, 1970; Rea and Naugler, 1971; Freedman and Parsons, 1986; Sager and Pringle, 1987; Pringle Jr, 1992; Kopp et al., 2003; O'Connor et al., 2015; Sotomayor et al., 2023). The MSP is situated south of the Pioneer fracture zone and northwest of the Hawaiian Islands and comprises ~420,000 km^2 of seafloor (Fig. 1). Previous authors have interpreted the following subregions/trends of

* Corresponding author.
E-mail address: Andrea.Balbas@csulb.edu (A. Balbas).

https://doi.org/10.1016/j.margeo.2023.107166
Received 17 August 2023; Received in revised form 8 October 2023; Accepted 13 October 2023
Available online 14 October 2023

the MSP:

(1) The western portion of the MSP is defined by a NW-SE (~327-degree striking) Cretaceous seamount chain. The chain is comprised of generally age-progressive seamounts, spanning from 98 Ma in the northwest to 80 Ma in the southeast (Sager and Pringle, 1987; Pringle Jr, 1992; O'Connor et al., 2015). The chain is thought to have initiated or became first expressed on the Pacific Plate at ~98 Ma, just south of the Pioneer fracture zone when the Pacific lithosphere began to drift over the Euterpe Plume (Sager and Pringle, 1987; Pringle Jr, 1992; Kopp et al., 2003). When plate reconstructions are employed to determine the latitude and longitude where the Musician Seamounts would have formed (e.g. hotspotting or backtracking; Wessel and Kroenke, 1997), the seamounts do not correlate to a region of the Pacific with active volcanism. Therefore, the Euterpe Plume is inferred to be extinct (Sager and Pringle, 1987; Wessel and Kroenke, 2008; Torsvik et al., 2019). It is currently uncertain how long the Euterpe plume has existed, as the southern extent of the age-progressive seamount chain is ambiguous due to overprinting by the Hawaiian plume and limited sampling among the South Hawaiian Seamounts (e.g., Sager and Pringle, 1987; Fig. 1).

(2) A series of large *E*-W striking volcanic elongated ridges (VERs) dominate the eastern portion of the MSP (Rea and Naugler, 1971; Kopp et al., 2003). These VERs range from small volcanic features to elongated rifts >400 km in length. The vertical profile of the ridges includes distinct peaks and valleys, with the peaks extending to a maximum of 3500 m above the surrounding seafloor (Kopp et al., 2003). The ridges include at least two flat-topped edifices, both residing at depths of 2700 mbsl. The Euterpe hotspot has been hypothesized to be at least partially responsible for the formation of the E-W trending VERs that extend from the seamount chain towards the ancient Pacific-Farallon spreading centers (Kopp et al., 2003). Kopp et al. (2003) proposed that the formation of channelized melt conduits between the rigorously upwelling MOR and the Euterpe Plume resulted in the VERs. Alternatively, Pringle Jr (1992) postulated the VERs formed as a result of melt migration along lithospheric tensional cracks. The VERs, particularly in the southern MSP, contain multiple gravity field flexural signatures indicating that volcanism was unusually long-lived or formed in multiple pulses (Freedman and Parsons, 1986). More recent pulses of volcanism were later confirmed by the discovery of multiple 47–50 Ma lava flows erupted along the southern VERs as well as along a scarp within the Murray fracture zone (O'Connor et al., 2015). This pulse of reactivated Eocene volcanism has been interpreted to be related to plate extension in the region during the ca. 50 Ma change in Pacific plate motion (O'Connor et al., 2015).

(3) The southernmost MSP region has been interpreted to contain seamounts that were driven by either continual diffuse extensional processes or shear-driven asthenospheric upwelling – producing the generally *E*-W trending roughly age progressive Naifeh, Plumeria and Mendelssohn seamount chains during the ~88–80 Ma timeframe (Sotomayor et al., 2023; Fig. 1, 2). A modern analog for this type of environment exists along the 20°S to 13°S East Pacific Rise (EPR). In this region there are numerous ridges and low volume seamounts that formed perpendicular to the spreading center and contain age progressions more in line with spreading rate than with plate motion (e.g. the Rano Rani, Sojourn and Pukapuka ridges; Sandwell et al., 1995; Janney et al., 2000; Ito and van Keken, 2007; Ballmer et al., 2013). Given the similarity in geometry and age patterns, it is plausible that many of the seamounts and ridges in the southern MSP are related to processes forming features like the Pukapuka Ridge as opposed to being derived from the Euterpe Plume (Sotomayor et al., 2023).

Complicating the understanding of the MSP is the lack of paleomagnetic constraints and geochronologic data from the underlying crust

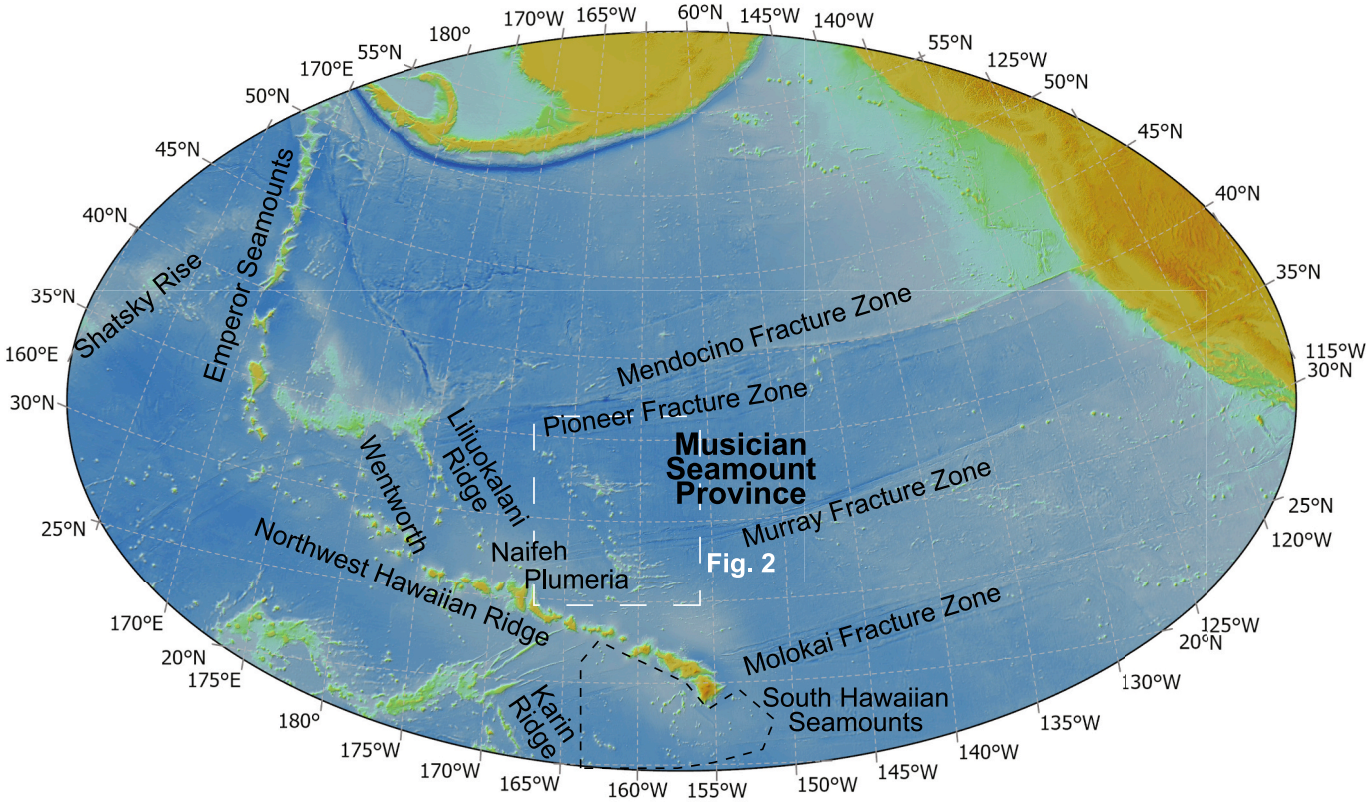

Fig. 1. A map of the mid to north Pacific with key features labeled. The extent of the Fig. 2 is noted.

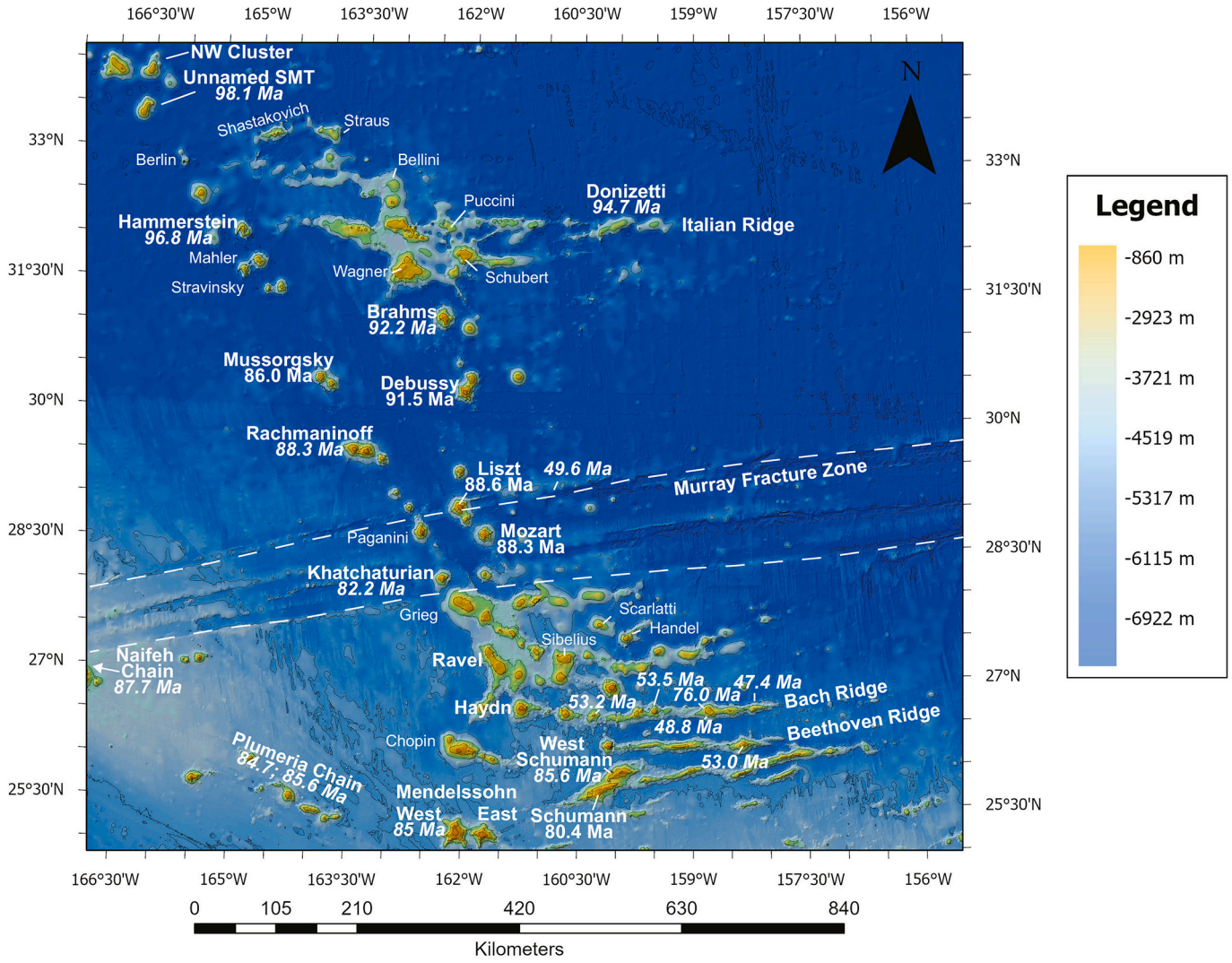

Fig. 2. Regional map of the MSP. Bathymetry from the GEBCO Bathymetric Compilation Group (2022). Represented ages are shown when multiple age determinations exist for a single feature (e.g. Bach Ridge). Ages shown are from this study as well as Pringle Jr (1992) and O'Connor et al. (2015) (italicized text).

(Sager and Pringle, 1987). The lithosphere in the region formed during the Cretaceous normal superchron (C34n, 121.4–83.65 Ma; Ogg, 2020), with the exception of C33r found at the easternmost tip of the southern VERs. Therefore, direct sampling and high-resolution age determinations for lava flows are required to interpret the region. The MSP hosts a range of plate and plume processes that make it an ideal natural environment to understand the range of volcanic dynamics that can drive topography in the ocean basins. The general age range of the MSP suggests it can offer new insights regarding Pacific plate motion at the time. Here we present new $^{40}Ar/^{39}Ar$ age determinations on lava flows collected from the MSP and provide novel insights into the formation of the MSP as well as its potential use in constraining Pacific plate motion in the late Cretaceous.

3. Methods

Samples used in this study were collected during the U.S. National Oceanic and Atmospheric Administration Ocean Exploration (NOAA-OER) expedition EX1708 (The Deep-Sea Symphony; Cantwell, 2020). Expedition EX1708 recovered in-situ geologic samples from eighteen seamounts and ridges in the MSP using the remotely operated vehicle (ROV) *Deep Discoverer*. Recovered geologic samples were cut, described and made available by the Oregon State University Marine Geology Repository. Table 1 shows the location of the ten lava flow samples selected for this study that were deemed to have phases suitable for $^{40}Ar/^{39}Ar$ age determination experiments.

The target phases for $^{40}Ar/^{39}Ar$ age determinations from lava samples were plagioclase and holocrystalline groundmass. The samples were crushed, washed, and sieved to the desired grain size and select phases were concentrated using magnetic sorting. The concentrated phases were then subjected to consecutive one-hour 50 °C ultrasonicated acid baths (3N HCl; 6N HCl; 1N HNO_3; 3N HNO_3) to remove secondary clay and carbonate alteration present following the methods outlined in Balbas et al. (2016) and Konrad et al. (2018). Plagioclase separates were given an additional 10 to 15 min bath in 4% HF to remove any sericite rims. The desired phases were then hand-picked for purity and homogeneity. The samples were wrapped in Al foil and packed into a quartz tube, along with standards of a known fluence age (Fish Canyon Tuff sanidine). All samples were then irradiated in the Oregon State University TRIGA reactor for six hours.

Analyses were conducted with the incremental heating method using a double-vacuum furnace attached to a stainless-steel extraction line at the Nevada Isotope Geochronology Laboratory (NIGL). Gases were exposed to a hot SAES 'getter' during fourteen minutes of furnace heating followed by an additional six-minute exposure to a second set of room temperature and hot SAES 'getters'. Processed gas was inlet into a NGX multi-collector noble gas mass spectrometer with ATONA amplifiers and time zero was initiated after a 20s equilibration time. The *m/z*

Table 1
Ages summary table.

Summary of $^{40}Ar/^{39}Ar$ Age Results for EX1708						Plateau								Inverse Isochron				
Sample	Seamount	Lat	Long	Phase	Age	Age	±2σ (i)	±2σ (f)	^{39}Ar	K/Ca	±2σ	MSWD	P	n	N	$^{40}Ar/^{36}Ar$	±2σ	SF	MSWD	P
Name					Type											intercept				
EX1708 - Musician Seamounts																				
EX1708-D05–1	Gounod	27.84	−161.29	PLG	No Age															
EX1708-D05–3	Gounod	27.84	−161.29	PLG	No Age															
EX1708-D07–2	Debussy	30.34	−162.05	PLG	Plateau	91.45	± 0.44 Ma	± 3.78 Ma	75%	0.017	± 0.001	1.43	16%	11	16	297.7	± 21.16	21%	1.59	11%
EX1708-D12–1	Mussorgsky	30.44	−164.01	PLG	Plateau	86.00	± 0.45 Ma	± 3.56 Ma	96%	0.014	± 0.001	1.39	16%	13	16	296.34	± 17.34	30%	1.50	12%
EX1708-D14–1	Liszt	28.96	−162.07	PLG	Plateau	88.61	± 0.71 Ma	± 3.70 Ma	85%	0.013	± 0.002	0.76	69%	13	15	294.9	± 1.77	89%	0.86	58%
EX1708-D15–6	Mozart	28.69	−161.67	PLG	Plateau	88.27	± 0.59 Ma	± 3.67 Ma	70%	0.014	± 0.001	1.62	11%	9	16	296.25	± 29.81	37%	1.83	8%
EX1708-D17–1	Haydn	26.61	−160.67	GM	No Age															
EX1708-D17–4	Haydn	26.6	−160.67	GM	No Age															
EX1708-D18–1	Schumann	25.76	−160.06	PLG	Plateau	80.40	± 0.40 Ma	± 3.32 Ma	74%	0.014	± 0.000	0.38	93%	9	16	297.46	± 2.43	51%	0.32	95%
EX1708-D19–2	Mendelssohn	25.16	−161.65	PLG	No Age															

PLG = plagioclase; GM = groundmass; n = heating steps used in age calculations.
i = internal uncertainty; f = full uncertainty; N = total heating steps analyzed.
P = probability of fit factor; SF = spreading factor.
MSWD = Mean square of the weighted deviants.

40, 39, 38, and 37 peaks were measured using faraday cups while the 36 peak was measured using an ion counter. Mass signal intensities were determined by regressing 150 three second peak integrations to time zero. A series of six to eight furnace hot blanks were run prior to the sample analyses and blank values were assigned based on step temperature using a polynomial fit to the blank results. Mass discrimination factor (MDF) values for each sample were calculated by fitting a polynomial curve through the air standard results (assuming a $^{40}Ar/^{36}Ar_{atm}$ of 298.56; Lee et al., 2006) run daily during the course of the experiments. Collector calibrations were determined after each MDF experiment by leaving the gas in the mass spectrometer and starting a new analysis where the 36 m/z peak was repeatedly alternated between the ion counter and neighboring faraday cup using peak hopping. Interfaraday peak intensity variability was determined to be negligible when ATONA gain calibrations are run monthly – consistent with NGX observations from other labs (e.g. Mixon et al., 2022). All age determinations were calculated using ArArCalc software (Koppers, 2002) assuming a Fish Canyon Tuff fluence monitor age of 28.201 Ma (Kuiper et al., 2008) and the decay constants of Min et al. (2000). Uncertainties are reported herein at the 2σ level and include propagated error on the individual peak regressions, temperature blank polynomial fits, MDFs, collector calibrations, irradiation constants, the J value curve and post irradiation decay of ^{37}Ar and ^{39}Ar. Additional uncertainties on the ^{40}K decay constant, natural element abundances and fluence monitor age are included with the external uncertainties (Supplemental Document). A statistically valid age was defined as having a plateau defining >50% of the $^{39}Ar_K$ released and containing a probability of fit factor > 0.05 (Table 1).

4. Results

Out of the ten experiments attempted, five produced concordant plateaus or isochrons (Table 1, Fig. 3). Samples EX1708-D05–1 and EX1708-D05–3 were collected from near the summit of Gounod seamount (pink dots; Fig. S6). Both lava flows contained abundant coarse grain plagioclase phenocrysts and an altered groundmass (Table S1). Plagioclase separates from each of these samples produced discordant heating spectrums (Fig. 3), therefore no age results are reported. The plagioclase basalt sample EX1708-D07–2 was collected from near the summit of Debussy seamount (Fig. S2). Plagioclase from this sample provided a concordant plateau with 75% of ^{39}Ar released and a plateau age of 91.45 ± 0.44 Ma (Fig. 3). An alkalic plagioclase-clinopyroxene-spinel phyric basalt (EX1708-D12–1) was collected from near the summit of Mussorgsky seamount (Fig. S1) and a plagioclase separate provided a concordant plateau with 96% of ^{39}Ar released, corresponding to an age of 86.00 ± 0.45 Ma (Fig. 3).

Sample EX1708-D14–1 is a plagioclase basalt that was collected from the flank of Liszt seamount (Fig. S4). A plagioclase separate experiment produced a concordant isochron with a slightly subatmospheric initial $^{40}Ar/^{36}Ar$ (294.9 ± 0.3; 85% of ^{39}Ar released). The plateau age was recalculated assuming the new $^{40}Ar/^{36}Ar_{int}$ value (and propagated uncertainty) to provide a concordant plateau with an age of 88.61 ± 0.71 Ma (Fig. 3). The plagioclase-olivine basalt EX1708-D15–6 was collected from the deep flank of Mozart seamount (Fig. S5). The plagioclase experiment produced a concordant age plateau corresponding to an age of 88.27 ± 0.59 Ma (Fig. 3). The lava flow samples EX1708-D17–1 and EX1708-D17–4 were collected from near the summit of Haydn seamount (Fig. S7). Both samples displayed a pattern indicative of partial degassing or silicate recrystallization at low temperature (young apparent ages), followed by an increase in apparent ages, then a continual decrease. Thus, no statistically valid age resulted from the analyses of these samples. A plagioclase separate from sample EX1708-D18–1 (collected from Schumann summit; Fig. S8) provided a concordant plateau (74% of 39Ar released) corresponding to an age of 80.40 ± 0.40 Ma (Fig. 3). No statistically valid age resulted from the analysis of sample EX1708-D19–2 that was collected from near the summit of

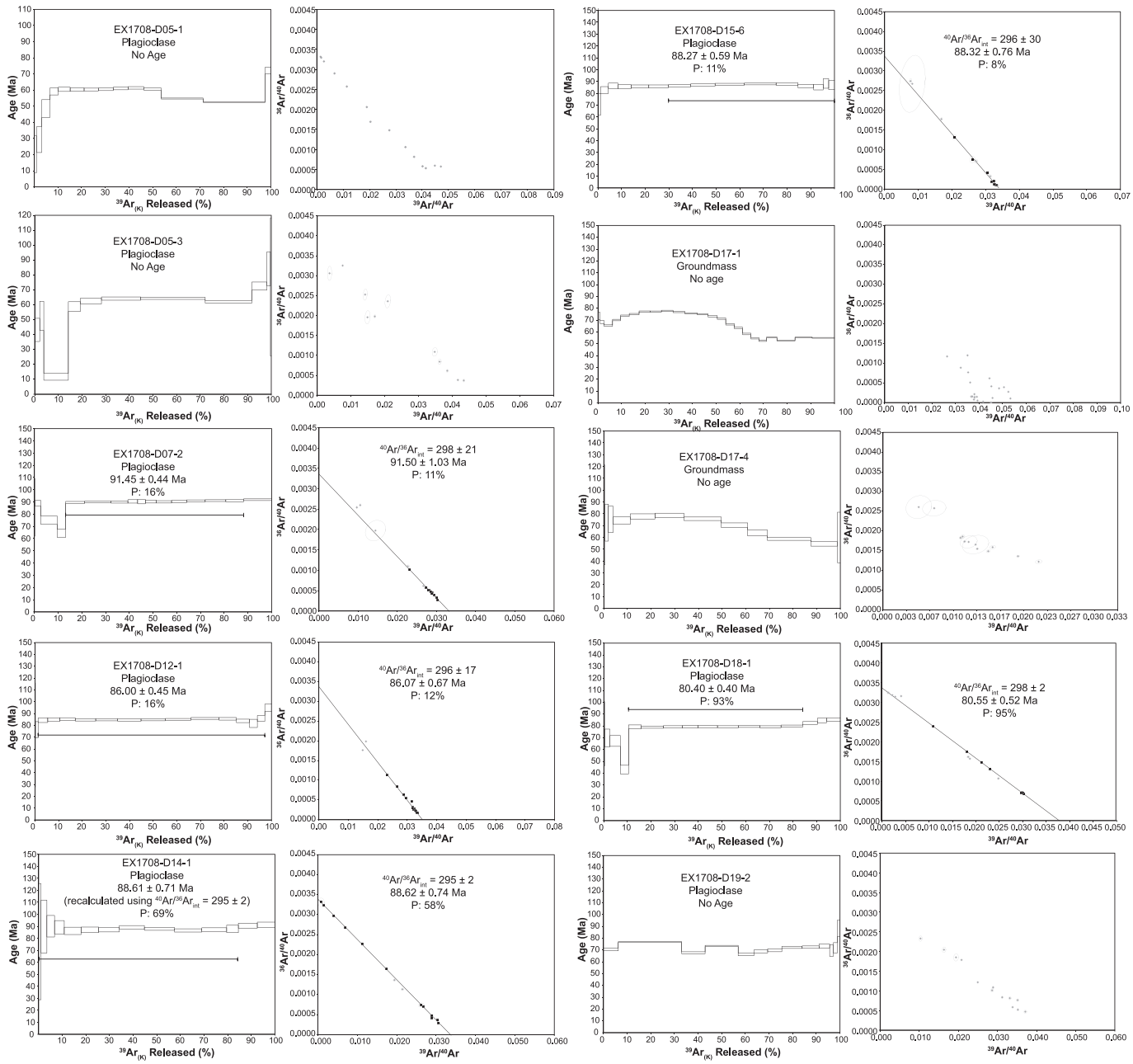

Fig. 3. Incremental heating $^{40}Ar/^{39}Ar$ age determinations and inverse isochron experiment results for the recovered EX1708 lava flows. The plateau for EX1708-D14–1 is recalculated using the slightly sub-atmospheric initial $^{40}Ar/^{36}Ar$ shown in the isochron. The probability of fit factors (P) are shown where a value >5% indicates statistical concordance of the population.

Mendelssohn seamount (Fig. S9).

5. Discussion

The new incremental heating $^{40}Ar/^{39}Ar$ age determinations are consistent with previous constraints (Sager and Pringle, 1987; Pringle Jr, 1992; O'Connor et al., 2015) but provide generally older ages for seamounts, particularly in the northern MSP. In order to better constrain the various processes that influenced this dynamic region, all previous age determination data needs to be filtered to meet modern $^{40}Ar/^{39}Ar$ quality control standards (e.g. Schaen et al., 2021). Accordingly, we have assessed and filtered all previous constraints from the region with brief sample justifications (Table 2). Furthermore, the $^{40}Ar/^{39}Ar$ ages presented and discussed have all been recalculated to the same fluence monitor (FCT sanidine; 28.201 Ma; Kuiper et al., 2008) and decay constants (Min et al., 2000). The K—Ar age determinations from Clague and Dalrymple (1975) are excluded here due to the unreliability of K—Ar for constraining the eruption ages of lava flows that have experienced aqueous alteration or potentially retained excess mantle ^{40}Ar during emplacement at high hydrostatic pressure (e.g. Pringle Jr, 1992). Fig. 2 includes the regional lava flow age determination data that meet modern criteria. Based on this dataset we provide a new reconciliation of the MSP history that identifies four distinct volcanic processes. This deconvolution of processes allows for the identification of age-progressive seamounts formed from the Euterpe plume that can be used to reconstruct plate motion during the late Cretaceous.

5.1. Origin of the Musician Seamount Province

Here we generate a new model for the evolution of the MSP using

Table 2
Musician Seamounts age evaluation.

Seamount	Lat	Long	Sample	Reference	Reliable	Justification
Name					Age	
NW Cluster	33.48	−166.53	KK804 1–9	Pringle Jr (1992)	Yes	Concordant
	33.48	−166.53	KK804 1–10	Pringle Jr (1992)	No	Discordant plateau; isochron MSWD somewhat high and not displayed anywhere
Hammerstein	32.47	−165.80	KK804 5–16	Pringle Jr (1992)	No	Only two steps on the plateau
	32.47	−165.80	KK8804 5–17	Pringle Jr (1992)	Yes	Only four steps but >50% ^{39}Ar and concordant
Mahler	31.63	−165.10	KK804 7–1	Pringle Jr (1992)	No	Does not meet minimum plateau length (>50% ^{39}Ar)
	31.63	−165.10	KK804 7–17	Pringle Jr (1992)	No	Visably Discordant Plateau; statistics not available
Rachmaninoff	29.55	−163.37	?	Sager and Pringle (1987)	Yes	TF plagioclase separates aren't ideal but the isochron has six points and is concordant
Liszt	28.97	−162.01	?	Pringle Jr (1992)	No	Only three discordant points
Haydn	26.63	−161.20	?	Pringle Jr (1992)	No	Only four points and discordant isochron
Khatchaturian	28.13	−162.28	A7-59D-15	Sager and Pringle (1987)	Yes	Concordant
	28.13	−162.28	A7-59D-31	Sager and Pringle (1987)	Yes	Concordant
Brahms	31.12	−162.36	KK804 21–6	Sager and Pringle (1987)	Yes	Concordant
East Mendelssohn	25.18	−161.60	KK807 37–2	Sager and Pringle (1987)	No	Three different acid treatments and all have three or less steps on the plateau
West Mendelssohn	25.13	−161.95	KK807 38–1	Sager and Pringle, 1987	No	Plateau does not appear concordant
	25.13	−161.95	KK807 38–1	Sager and Pringle, 1987	Yes	Concordant
	25.13	−161.95	KK807 38–2	Pringle (1992)	No	No plateau developed
Central Bach Ridge	26.58	−158.83	KK807 27–2	Sager and Pringle (1987)	Yes	Plateau not ideal but likely concordant
	26.58	−158.83	KK807 27–3	Pringle Jr (1992)	No	Discordant plateau
West Schumann	25.95	−159.90	KK848 52-51 A	Sager and Pringle (1987)	Yes	Concordant
Donizetti	32.25	−159.95	SO142 4DR-3	O'Connor et al. (2015)	No	Mini-plateau (43%)
	32.27	−159.47	SO142 5DR-1	O'Connor et al. (2015)	Yes	Just barely a useable plateau (50%)
Murray Ridge	29.26	−160.41	SO142 6DR-1	O'Connor et al. (2015)	Yes	Concordant
Murray Ridge	29.29	−160.41	SO142 6DR-4	O'Connor et al. (2015)	Yes	Concordant
Bach Ridge	26.62	−160.26	SO142 8DR-1	O'Connor et al. (2015)	Yes	Same separate as other Bach samples
Bach Ridge	26.62	−160.26	SO142 8DR-1	O'Connor et al. (2015)	Yes	Same separate as other Bach samples
Bach Ridge	26.62	−160.26	SO142 8DR-1	O'Connor et al. (2015)	Yes	Same separate as other Bach samples
Bach Ridge	26.62	−160.28	SO142 8DR-3	O'Connor et al. (2015)	No	Discordant
Bach Ridge	26.62	−160.28	SO142 8DR-3	O'Connor et al. (2015)	Yes	Concordant
Bach Ridge	26.66	−159.48	SO142 9DR-1	O'Connor et al. (2015)	Yes	Concordant
Bach Ridge	26.66	−159.48	SO142 9DR-1	O'Connor et al. (2015)	Yes	Concordant
Bach Ridge	26.56	−158.79	SO142 10DR-2	O'Connor et al. (2015)	Yes	Concordant
Bach Ridge	26.56	−158.79	SO142 10DR-2	O'Connor et al. (2015)	Yes	Concordant
Bach Ridge	26.56	−158.79	SO142 10DR-2	O'Connor et al. (2015)	Yes	Concordant
Bach Ridge	26.58	−158.79	SO142 10DR-4	O'Connor et al. (2015)	Yes	Concordant
Bach Ridge	26.58	−158.79	SO142 10DR-4	O'Connor et al. (2015)	Yes	Concordant
Bach Ridge	26.58	−158.79	SO142 10DR-4	O'Connor et al. (2015)	Yes	Concordant
Bach Ridge	26.71	−158.24	SO142 12DR-1	O'Connor et al. (2015)	Yes	Concordant
Bach Ridge	26.71	−158.24	SO142 12DR-1	O'Connor et al. (2015)	Yes	Concordant
Bach Ridge	26.71	−158.24	SO142 12DR-1	O'Connor et al. (2015)	Yes	Concordant
Beethoven Ridge	26.16	−158.42	SO142 13DR-2	O'Connor et al. (2015)	Yes	Concordant
Beethoven Ridge	26.16	−158.42	SO142 13DR-2	O'Connor et al. (2015)	Yes	Concordant

new and previous chronologic constraints from the region. Fig. 4 shows the temporal evolution of the MSP in four time slices. The reconstructed latitude/longitudes are approximate as each available Pacific APM model predicts a different plume location and no current model perfectly fits the observed data (Fig. 5). In this model, we hold the Euterpe plume fixed and assume no motion due to plume-ridge capture or release (e.g. Tarduno et al., 2003). The ridge and transform fault (TF) locations are best estimates and become more detailed after the end of C34n, where crustal magnetic isochrons can be traced (Fig. 4D). Below we discuss the temporal evolution of the four proposed features/drivers of volcanism in the MSP.

5.1.1. *Euterpe Hotspot track*

The MSP initiates immediately south of the Pioneer fracture zone (Figs. 1, 4A) as a cluster of four small seamounts. One of the unnamed seamounts was dredged and a recovered trachyte produced a concordant

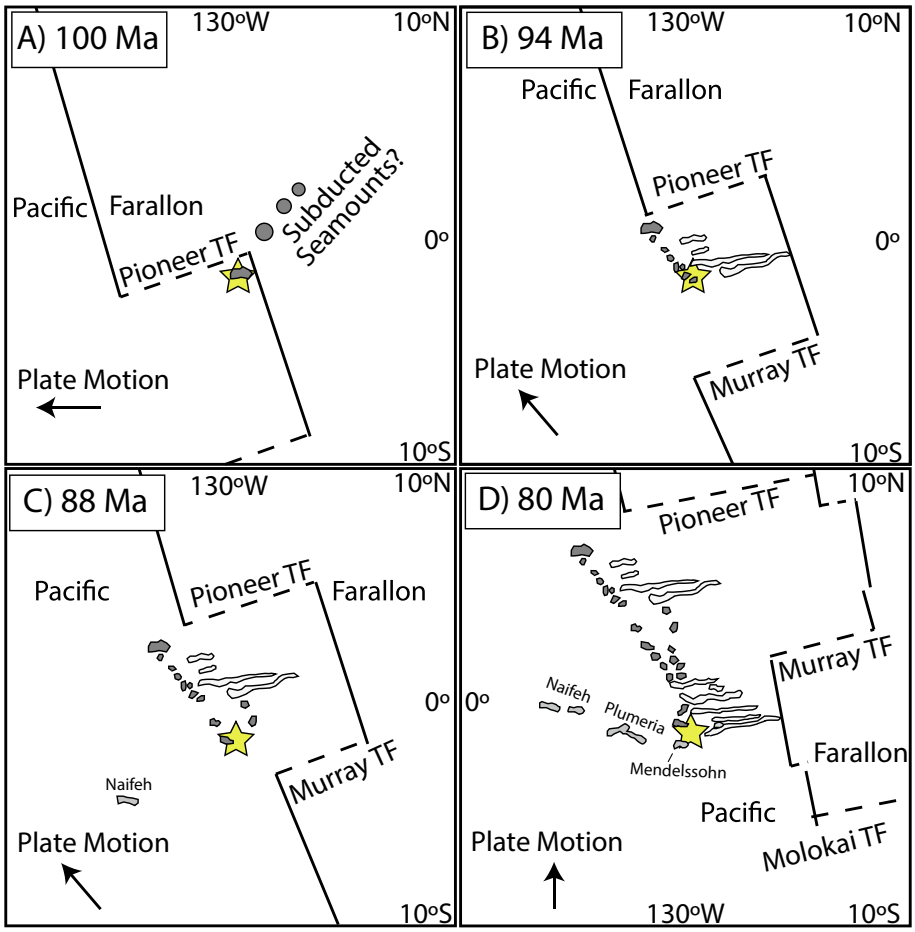

Fig. 4. A schematic evolution of the Musician Seamount Province in 6 Ma time slices. The yellow star is the location of the Euterpe plume, black lines are the spreading center axes, the dashed lines are transform faults (TF), dark grey shapes are the Euterpe plume related volcanic features, white infill represents VER formation and light grey are seamounts formed from other processes (e.g. Sotomayor et al., 2023). (A) The change in plate motion at ca. 100 Ma results in the Pacific lithosphere moving over the Euterpe plume. Any evidence of the seamount chain on the Farallon plate would have been subducted. (B) Plume-ridge channelization results in the generation of a series of VERs that grow progressively longer as the ridge moves further from the hotspot. (C) After separating a distance >600 km from the ridge, the plume-ridge channels end and a dual track hotspot track emerges. (D) Once the Murray fracture zone passes near the hotspot at ~86 Ma, the ridge becomes closer and VERs begin to be generated again, progressively growing longer as the ridge moves from the hotspot. At 82–80 Ma, plate motion vectors change the plume-ridge channelization ends once more.

age of 98.1 Ma (Pringle Jr, 1992). Provided that the western edge of the MSP was sourced by the fixed Euterpe plume (Pringle Jr, 1992; Kopp et al., 2003; O'Connor et al., 2015), the change in plate vectors associated with the 105–100 Ma global plate reorganization event (GPRE; e.g. Matthews et al., 2012) would have resulted in the surface expression of the plume shifting from the Farallon plate (which is now subducted) to the Pacific plate (Sager and Pringle, 1987; Fig. 4A). Once present beneath the Pacific plate, the plume generated an age-progressive seamount chain. The co-polar Liliuokalani Ridge, Karin Ridge and Wentworth Seamounts (Fig. 1) indicate that the geometry of the western MSP seamounts mirror late Cretaceous Pacific plate motion.

The western MSP seamount trend continues to become younger towards the SE. This includes the Mussorgsky (86 Ma), Rachmaninoff (88.3 Ma; Sager and Pringle, 1987), and Khatchaturian (82.2 Ma; Sager and Pringle, 1987) seamounts. It is important to note that seamounts can typically exist for up to 4–7 Myrs and that post-erosional volcanic products can cover the summits of seamounts/islands (e.g. Konter et al., 2009; Clague and Sherrod, 2014; Heaton and Koppers, 2019). The deep flanks of seamounts are typically considered the best sample locations for constraining the time of the shield-building stage, when the seamount is most likely to have been overriding the central hotspot axis (Koppers et al., 2011; Konrad et al., 2018). The lava flow from Mussorgsky (EX1708-D12–1; 86 Ma) was recovered from the summit of the seamount and likely represent late-stage or rejuvenated volcanism. In contrast, dredge samples from the flanks of Rachmaninoff seamount, which resides 900 km to the SE of Mussorgsky, displayed concordant $^{40}Ar/^{39}Ar$ total fusion ages of 88 Ma (Sager and Pringle, 1987). Accordingly, we focus on the older seamount ages from a chain when constraining plate velocities.

The age progressions are relatively consistent until Haydn seamount (26.6 N, 161.2 W) where the trend becomes more convoluted (Fig. 2). In the southern most region, the hotspot may have directly sourced the Schumann (80.4 Ma), West Schumann (85.6 Ma; Pringle, 1992) and/or West Mendelssohn (84.9 Ma; Sager and Pringle, 1987) seamounts. Most Pacific rotation poles and associated local plate velocities (e.g., Duncan and Clague, 1985; Wessel and Kroenke, 2008; Torsvik et al., 2019; Müller et al., 2019) for the MSP region would predict a fixed Euterpe hotspot underlying the southern MSP (e.g., ~25.5 N; 161.5 W) at ~77–80 Ma (Fig. 5B). These predictions are in line with the younger Schumann seamount age of 80 Ma and the Central Bach Ridge age of 76 Ma (O'Connor et al., 2015). In this scenario, the dated Mendelssohn and West Schumann lava flows would have been emplaced prior to the lithosphere overriding the hotspot. Sotomayor et al. (2023) proposed that Mendelssohn formed from the same shear-driven upwelling or diffuse extensional processes that sourced the Naifeh and Plumeria chains (Fig. 1). We propose that it is possible that part or all of West

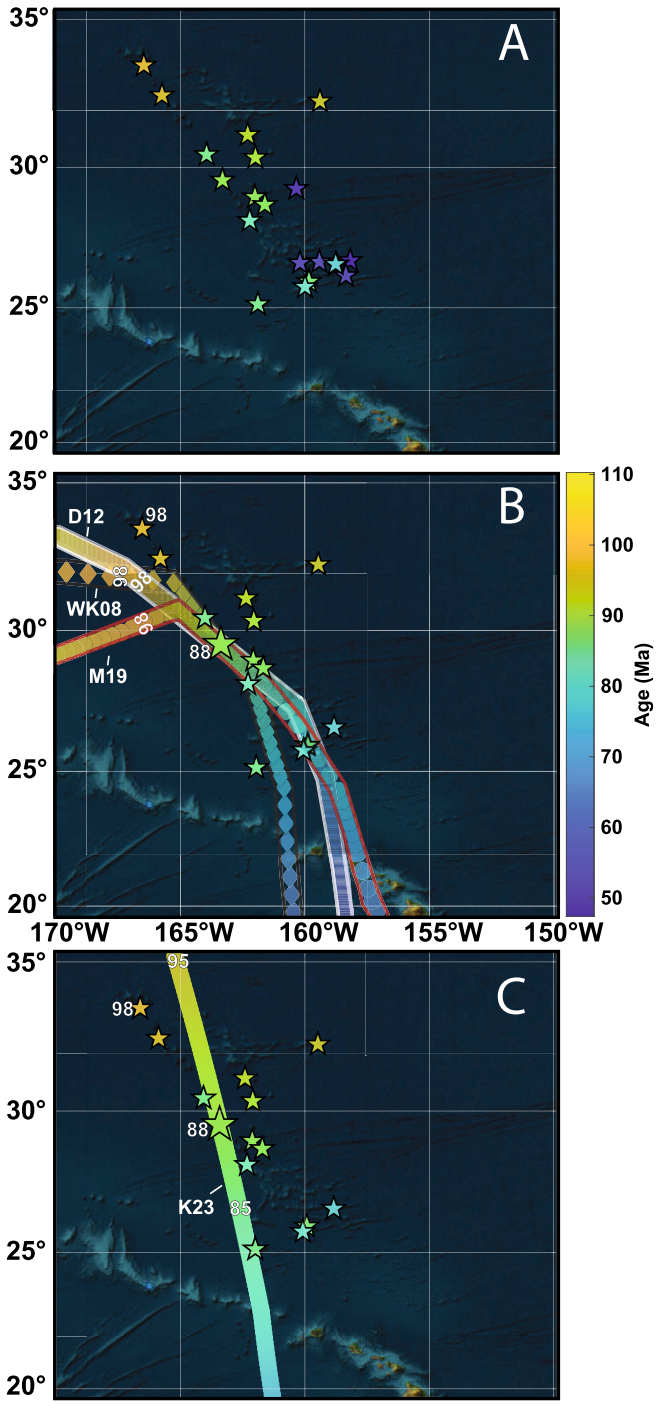

Fig. 5. The comparison of Pacific plate motion mantle flowline models to the observed distribution of ages in the MSP. (A) All the filtered lava flow age determinations (stars). (B) The paths of the fixed hotspot model of Wessel and Kroenke (2008) (WK08; black outline), the mobile hotspot model of Doubrovine et al. (2012) (D12; white outline) and the global plate-circuit model of Müller et al. (2019) (M19; red outline). These flowlines are rooted to the 88 Ma Rachmaninoff seamount (Pringle Jr, 1992). (For interpretation of the references to colour in this figure legend, the reader is referred to the web version of this article.)

Schumann seamount formed from those same process(es).

An alternate scenario, wherein West Schumann and Mendelssohn track the timing of the Euterpe plume, can be supported by the recent APM model of Konter et al. (2023). This model is a modification of Koppers et al. (2001), wherein more rapid angular velocities are assumed at 100–80 Ma in order to fit isotopically similar Western Pacific Seamount Province lava flows to the active Samoa and Rurutu-Arago plumes. Although the proposed model is a first-order assessment based on limited age determinations, the corresponding faster plate velocities predict the Euterpe plume would override the southern MSP at ca. 84 Ma (Fig. 5C).

Whether the plume dies out at ~80 Ma, or continues south of the Hawaiian Ridge is currently unknown. The Konter et al. (2023) and Wessel and Kroenke (2008) models predict that the seamount chain would follow a southern trajectory, sourcing the less concordant ca. 80 Ma lava flow age determinations for Mendelssohn W and E (Sager and Pringle, 1987) before potentially sourcing the uncharacterized, N-S trending Chautauqua Seamounts (~22°N, 162.5°W; Fig. 1). Alternatively, the Doubrovine et al. (2012) and Müller et al. (2019) rotation poles predict the hotspot track would continue to the SE, potentially sourcing some of the South Hawaiian Seamounts in the 55–65 Ma timeframe. Ultimately, coupling isotopes with age determinations in the MSP and among the South Hawaiian Seamounts will be needed to trace the southern extent and path of the Euterpe hotspot.

5.1.2. *Volcanic elongated ridges*

As the hotspot 'jumped' from the Farallon to Pacific plate at ca. 100 Ma, it was initially positioned near the ancient Pacific-Farallon spreading center. This resulted in channels of melt being entrained between the hotspot and ridge, generating small seamounts that grew together into larger ridge like structures (VERs; e.g. Kopp et al., 2003). A modern example for this plume-ridge melt channelization mechanism is the Wolf-Darwin lineament, which is a series of small seamounts that extend from the active Galapagos hotspot to the neighboring spreading center (e.g., Morgan, 1978; Mittal and Richards, 2017). A prevailing model to explain the origin of these VERs invokes asthenospheric flow fueling buoyant melt through channels leading away from the hotspot towards the spreading center (Mittal and Richards, 2017), however, tensional stress from the local transform fault-ridge corner may be required to drive the volcanism (Harpp and Geist, 2002). The northern MSP contains approximately four VERs that become progressively longer towards the south (Fig. 4B). The length of individual Musician VERs are likely a function of the distance between the hotspot and the ridge at the time of formation. The relative vectors between a NW moving Pacific plate and westward crustal growth would result in the ridge becoming systematically further from the hotspot through time. The eastern edge of the longest northern VER (Donizetii seamount on the Italian Ridge) was dredged, with a lava flow producing an age of 94.7 Ma (O'Connor et al., 2015; Fig. 2). This VER age is consistent with the age progressions along the western MSP. These observations suggest that a plume-ridge distance of 500–600 km may be the upper limit to maintain a channelized melt conduit in this scenario. The maximum length of the VER's in the MSP is 500–600 km, which is the distance from the modeled plume center to the opposing end of Italian Ridge. This is shorter than the proposed potential length of VER's (~1000 km) modeled by Mittal and Richards (2017) but may represent the maximum length possible given the size and buoyancy of the Euterpe plume at ca. 95 Ma.

The VERs abruptly disappear south of the Italian Ridge and instead a few scattered seamounts are present (Figs. 2, 4C). Brahms (92.2 Ma; O'Connor et al., 2015) and Debussy (91.45 Ma) seamounts are temporally consistent with age-progressions expected from the Euterpe plume. These seamounts may relate to plume-ridge channelization but their distances from the main seamount track (150–170 km) are not significantly different from other broad seamount chains with dual trends (e.g. Marquesas Islands; Hawaii) and as such may represent distinct melt

conduits forming over a broad plume (e.g., Chauvel et al., 2012; Jones et al., 2017). The distance between the dual trends of seamounts decreases continually towards the Murray fracture zone (Fig. 2). The Murray fracture zone in the MSP region is ~100 km wide and contains three distinct horst and grabens. However, there is no offset in the seamount orientations across the zone, which indicates the transform fault was not active while the hotspot underlaid the feature (Sager and Pringle, 1987).

Immediately south of the Murray fracture zone, the VERs fully reappear (Fig. 2; Fig. 4D). This observation is consistent with VER formation by plume-ridge channelization. South of the Murray fracture zone, the lithosphere is younger and thus the paleo-ridge would have been closer (within 500 km) to the Euterpe hotspot. The decreased plume-ridge distance would have allowed for melt channels to form once more. The VERs become continually longer towards the south, ending with the southernmost ridge (Blackfin). Blackfin Ridge extends to a length of 400 km from Schumann seamount (Fig. 2). Further supporting that the southern MSP lithosphere overlaid the Euterpe plume at ca. 80 Ma (as discussed in section 5.1.1) is the appearance of C33n (79.9 Ma; Atwater and Severinghaus, 1989; Ogg, 2020) at the easternmost tip of Schumann ridge. This temporally connects the ancient spreading center with Schumann seamount (80.4 Ma), providing strong support for both the plume location and the plume-melt channelization hypothesis (Kopp et al., 2003).

5.1.3. Non-Euterpe Plume Derived Volcanism

Moving southwards from the Murray to the Molokai fracture zone, the morphology of the VERs change from linear chains of small seamounts to more elongated steeply sloped ridges (Fig. 2). Among the southern VERs, numerous 54–47 Ma lava flows were recovered (O'Connor et al., 2015). These lava flows were believed to be emplaced as a function of lithospheric extension associated with the well-established change in Pacific plate vectors at the time (Torsvik et al., 2017; Finlayson et al., 2018; Gaastra et al., 2022). The Cretaceous aged lava flows recovered from the Bach and Schumann ridges indicate that the VERs were likely initially emplaced during the Cretaceous and then some conduits were re-occupied in the Eocene. Thus far, the reactivated volcanism seems constrained to the southernmost VERs and at least one location along the Murray fracture zone (O'Connor et al., 2015).

South of Beethoven Ridge, there are numerous very thin (5–10 km) ridges that generally trend perpendicular to the paleo-spreading center (Fig. 2). None of the small ridges or volcanic cones have been sampled and interestingly, the presence of numerous small ridges and seamounts are continuous within the lithospheric block situated south of the Murray fracture zone, north of the Molokai fracture zone and extending from the MSP to the North American plate border (Fig. 1). This infers that the features are likely directly related to local EPR processes, like continuous shear-driven upwelling (e.g. Sotomayor et al., 2023) or potentially this region of mid-Pacific lithosphere is particularly prone to lithospheric thinning/extension during changes in plate motion (e.g., Butterworth et al., 2014; O'Connor et al., 2015). Direct sampling is required to understand the origin of these features. In summation, the MSP formed from: (1) hotspot volcanism (Pringle Jr, 1992; Kopp et al., 2003; O'Connor et al., 2015), (2) hotspot-ridge channelization (Kopp et al., 2003), (3) regional extension or shear-driven upwelling (Sotomayor et al., 2023) and (4) reactivated late stage volcanism due to extension (O'Connor et al., 2015). These processes encompass over 50 Myrs of regional volcanic history, highlighting that complex topographic domains in the ocean basins can be derived by a range of processes. This suggests that detailed sampling, especially of low volume seamounts, is required to understand the complexities of intraplate volcanism.

5.2. New insights into Pacific Plate motion in the late cretaceous

Age-progressive seamount chains, sourced from presumed fixed (e.g. Duncan and Clague, 1985; Wessel and Kroenke, 2008; Konter et al., 2023) or mobile (e.g. Doubrovine et al., 2012) mantle plumes have long been used to constrain absolute plate motion. Given the complexities of the MSP, careful seamount and age selection is required when calibrating Pacific APM in the Late Cretaceous. The westernmost seamount chain is clearly co-polar to similar aged features (e.g. Karin Ridge; Davis et al., 2002) and consists of the NW Cluster (98.1 ± 0.8 Ma), Hammerstein (96.8 ± 2.5 Ma), Mussorgsky (86.0 ± 0.45 Ma), Rachminoff (88.3 ± 2.5 Ma), Liszt (88.61 ± 0.71 Ma), Mozart (88.27 ± 0.59 Ma), and Khatchaturian (82.2 ± 2.7 Ma), which are all clear candidates for fitting an age progressive geometry. However, it is important to reiterate that the dated lava flow from Mussorgsky was recovered near the summit and as such may represent late stage volcanism. The more easterly situated Brahms (92.2 ± 0.8 Ma) and Debussy (91.45 ± 0.44 Ma) Seamounts follow the same age progressions, are distinct seamounts as opposed to VERs and are close enough to the western chain that they should be employed as constraints. Since the southern MSP is more complex, further work is needed to best determine which of those seamounts can be used in APM models. In total, we assess that nine seamounts and their corresponding $^{40}Ar/^{39}Ar$ age determinations are valuable constraints for APM models (Figs. 5, 6). Below we use the seamounts to provide new constraints on local plate velocity and the timing of changes in Pacific plate motion.

A local plate velocity estimate for the 98 to ~81 Ma timeframe is constrained with seamount distances calculated relative to Ravel seamount (27°N, 161.5°W; red dot Fig. 5A). Ravel seamount is chosen as it approximately represents the location where the MSP appears to shift in orientation, transitioning from a NW-SE to a more N-S trend (Fig. 5A). The resulting local plate velocity of 42 ± 9 km/Ma is within uncertainty of previous estimates of 52.9 ± 5.8 km/Ma from Pringle Jr, 1992. Furthermore, a ca. 81 Ma age is modeled for the apparent change in plate motion vectors in the southern MSP. This change is supported by the limited age constrains among the northern Emperor seamount chain, which shows a similar bend just north of Detroit seamount (79 Ma; Duncan and Keller, 2004). Thus, the ca. 81 Ma bend is consistent with being a shift in Pacific rotation poles.

Current age constraints on the timing of Pacific plate pole shifts for the late Cretaceous GPRE are severely lacking. No $^{40}Ar/^{39}Ar$ measurements of seamount chains directly bracketing the plate motion event currently exist. The timing of the Pacific expression of the Mid-Cretaceous GPRE has been placed at 100 Ma, based on rough estimates of minimum seamount ages from carbonate paleontological evidence (Duncan and Clague, 1985). This rough timing has continued to be used in follow-up APM models either directly (Koppers et al., 2001; Steinberger and Gaina, 2007) or modified (Torsvik et al., 2019). Wessel and Kroenke (2008) attempted to calculate the age of the Pacific Plate motion shift based on available radiometric age constraints from seamounts that precede the bend, resulting in an age of 95 ± 8 Ma for the change in Pacific rotation poles. Since relative plate-circuit rotations for the Pacific through the Antarctic (± Zealandia) reference frame are only directly valid until 83 Ma (e.g. Matthews et al., 2016; Müller et al., 2016; Tetley et al., 2019), relative motions of the Pacific Plate become heavily model dependent and less constrained prior to 83 Ma (e.g. Chandler et al., 2012). Unfortunately, the MSP does not bracket the late Cretaceous GPRE, but the 98 Ma age for the NW Cluster provides an important constraint that the rotation has to have occurred prior to 98 Ma.

6. Conclusions

Our new age determinations, in reconciliation with previous data, show that volcanic rocks recovered from the MSP record four distinct processes. (1) The primary process is the upwelling Euterpe plume that produced the NW-SE trending age progressive seamount track. (2) Adjacent to many age-progressive seamounts, VER's extend towards a paleo-spreading center. It has been hypothesized that these VER's resulted from conduits of melt extending from the hotspot to the ancient

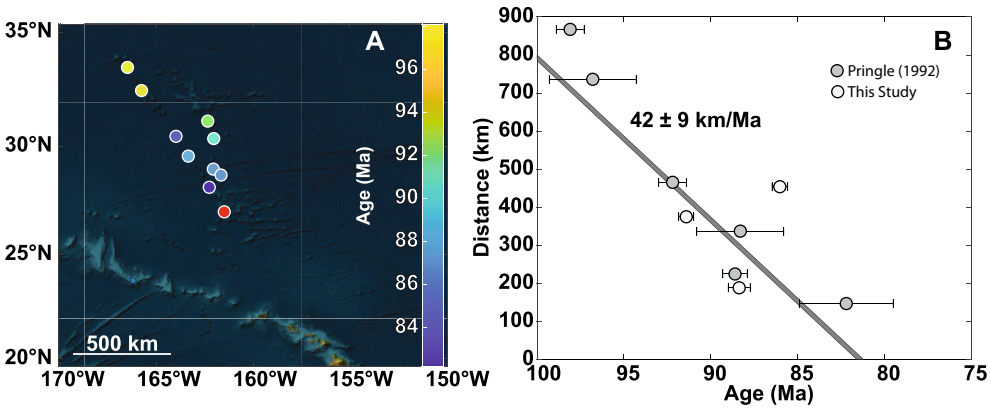

Fig. 6. The local plate velocity for the 100–80 Ma time frame as inferred by the Euterpe derived MSP chain. (A) The lava flows used in the calculation (circles) and the presumed 'bend' location that distances are calculated from (Ravel seamount; red dot). (B) The corresponding local velocity. (For interpretation of the references to colour in this figure legend, the reader is referred to the web version of this article.)

spreading center. The occurrence of the VER's appears to be controlled by the hotspots distance from the spreading center as they only occur during periods when the ridge and plume are within ~600 km or less from one another. (3) The regional reactivation of volcanism (after a period of ~30 Ma) associated with the Pacific plate reorientation in the Eocene is of limited volume and confined to southernmost MSP and the Murray fracture zone. (4) The 85–86 Ma lava flows present in the southernmost MSP are likely sourced from the same processes (shear-driven upwelling or diffuse extension) that generated the Naifeh and Plumeria chains to the west. Using lava flows most likely to be directly sourced from the Euterpe plume, we calculate a local plate velocity of 42 ± 9 km/Ma for the 98–81 Ma time frame (e.g. during primary MSP formation). The southern MSP appears to 'bend' at 81 Ma, consistent with previously proposed changes in Pacific rotation poles. The seamount age in the northernmost MSP indicates that the Pacific rotation associated with the late Cretaceous GPRE occurred prior to 98 Ma.

Declaration of Competing Interest

The authors declare the following financial interests/personal relationships which may be considered as potential competing interests:

Andrea Balbas reports financial support was provided by National Science Foundation.

Data availability

All samples from this study are archived at the Oregon State University Marine Geology Repository and are available upon request. Sample IGSN and metadata information available on SESAR. All age determination data is made available in the supplemental document.

Acknowledgements

We thank the captain and crew of the R/V *Okeanos Explorer* during expedition EX1708. The Oregon State University Marine Geology Repository is thanked for providing the samples analyzed in this study. We are grateful for the $^{40}Ar/^{39}Ar$ sample preparation and analytical assistance of Brandon Scott and Kathleen Zanetti. A Balbas and C Jung were supported by NSF-OCE #1936544. C Jung's CSULB MS thesis research constitutes much of the results presented here. We thank Brian Jicha and an anonymous reviewer for constructive feedback that improved this manuscript.

Appendix A. Supplementary data

Supplementary data to this article can be found online at https://doi.org/10.1016/j.margeo.2023.107166.

References

Atwater, T., Severinghaus, J., 1989. Tectonic maps of the Northeast Pacific the Geology of North America, N. In: Hussong, D.M. (Ed.), The Eastern Pacific Ocean and Hawaii EL Winterer. RW Decker, pp. 15–20.

Balbas, A., Koppers, A.A., Kent, D.V., Konrad, K., Clark, P.U., 2016. Identification of the short-lived Santa Rosa geomagnetic excursion in lavas on Floreana Island (Galapagos) by 40Ar/39Ar geochronology. Geology 44 (5), 359–362.

Ballmer, M.D., Conrad, C.P., Smith, E.I., Harmon, N., 2013. Non-hotspot volcano chains produced by migration of shear-driven upwelling toward the East Pacific rise. Geology 41 (4), 479–482.

Butterworth, N.P., Müller, R.D., Quevedo, L., O'Connor, J.M., Hoernle, K., Morra, G., 2014. Pacific plate slab pull and intraplate deformation in the early Cenozoic. Solid Earth 5 (2), 757–777.

Cantwell, K., 2020. Cruise Report: EX-17-08, Deep-Sea Symphony: Exploring the Musicians Seamounts (ROV & Mapping). https://doi.org/10.25923/pvw9-b391.

Chandler, M.T., Wessel, P., Taylor, B., Seton, M., Kim, S.S., Hyeong, K., 2012. Reconstructing Ontong Java Nui: implications for Pacific absolute plate motion, hotspot drift and true polar wander. Earth Planet. Sci. Lett. 331, 140–151.

Chauvel, C., Maury, R.C., Blais, S., Lewin, E., Guillou, H., Guille, G., Rossi, P., Gutscher, M.A., 2012. The size of plume heterogeneities constrained by Marquesas isotopic stripes. Geochem. Geophys. Geosyst. 13 (7).

Clague, D.A., Dalrymple, G.B., 1975. Cretaceous K-Ar ages of volcanic rocks from the Musicians Seamounts and the Hawaiian Ridge. Geophys. Res. Lett. 2 (7), 305–308.

Clague, D.A., Sherrod, D.R., 2014. Growth and Degradation of Hawaiian Volcanoes: Chapter 3 in Characteristics of Hawaiian Volcanoes (No. 1801-3, pp. 97-146). US Geological Survey.

Davis, A.S., Gray, L.B., Clague, D.A., Hein, J.R., 2002. The Line Islands revisited: New 40Ar/39Ar geochronologic evidence for episodes of volcanism due to lithospheric extension. Geochem. Geophys. Geosyst. 3 (3), 1–28.

Doubrovine, P.V., Steinberger, B., Torsvik, T.H., 2012. Absolute plate motions in a reference frame defined by moving hot spots in the Pacific, Atlantic, and Indian oceans. J. Geophys. Res. Solid Earth 117 (B9).

Duncan, R.A., Clague, D.A., 1985. Pacific plate motion recorded by linear volcanic chains. In: The Ocean Basins and Margins: Volume 7A the Pacific Ocean. Springer US, Boston, MA, pp. 89–121.

Duncan, R.A., Keller, R.A., 2004. Radiometric ages for basement rocks from the Emperor Seamounts, ODP Leg 197. Geochem. Geophys. Geosyst. 5 (8).

Dürkefälden, A., Geldmacher, J., Portnyagin, M., Garbe-Schönberg, D., Werner, R., Müller, D., Hauff, F., Hoernle, K., 2021. Papanin ridge and ojin rise seamounts (Northwest Pacific): dual hotspot tracks formed by the shatsky plume. Geochem. Geophys. Geosyst. 22 (9) p.e2021GC009847.

Finlayson, V.A., Konter, J.G., Konrad, K., Koppers, A.A.P., Jackson, M.G., Rooney, T.O., 2018. Sr–Pb–Nd–Hf isotopes and 40Ar/39Ar ages reveal a Hawaii–Emperor-style bend in the Rurutu hotspot. Earth Planet. Sci. Lett. 500, 168–179.

Freedman, A.P., Parsons, B., 1986. Seasat-derived gravity over the Musicians Seamounts. J. Geophys. Res. Solid Earth 91 (B8), 8325–8340.

Gaastra, K.M., Gordon, R.G., Woodworth, D.T., 2022. Quantification of Pacific Plate Hotspot Tracks since 80 Ma. Tectonics 41 (7) p.e2021TC006772.

GEBCO Bathymetric Compilation Group, 2022. The GEBCO_2022 Grid - a continuous terrain model of the global oceans and land. NERC EDS British Oceanogr. Data Centre NOC. https://doi.org/10.5285/e0f0bb80-ab44-2739-e053-6c86abc0289c.

Harpp, K., Geist, D., 2002. Wolf–Darwin lineament and plume–ridge interaction in northern Galápagos. Geochem. Geophys. Geosyst. 3 (11), 1–19.

Heaton, D.E., Koppers, A.A.P., 2019. High-resolution 40Ar/39Ar geochronology of the Louisville Seamounts IODP Expedition 330 drill sites: implications for the duration of hot spot-related volcanism and age progressions. Geochem. Geophys. Geosyst. 20 (8), 4073–4102.

Ito, G., van Keken, P.E., 2007. Hotspots and melting anomalies. Treat. Geophys. 7, 371–436.
Janney, P.E., Macdougall, J.D., Natland, J.H., Lynch, M.A., 2000. Geochemical evidence from the Pukapuka volcanic ridge system for a shallow enriched mantle domain beneath the South Pacific Superswell. Earth Planet. Sci. Lett. 181 (1–2), 47–60.
Jiang, Q., Jourdan, F., Olierook, H.K., Merle, R.E., Whittaker, J.M., 2021. Longest continuously erupting large igneous province driven by plume-ridge interaction. Geology 49 (2), 206–210.
Jones, T.D., Davies, D.R., Campbell, I.H., Iaffaldano, G., Yaxley, G., Kramer, S.C., Wilson, C.R., 2017. The concurrent emergence and causes of double volcanic hotspot tracks on the Pacific plate. Nature 545 (7655), 472–476.
Konrad, K., Koppers, A.A., Steinberger, B., Finlayson, V.A., Konter, J.G., Jackson, M.G., 2018. On the relative motions of long-lived Pacific mantle plumes. Nat. Commun. 9 (1), 854.
Konter, J.G., Staudigel, H., Blichert-Toft, J., Hanan, B.B., Polvé, M., Davies, G.R., Shimizu, N., Schiffman, P., 2009. Geochemical stages at Jasper Seamount and the origin of intraplate volcanoes. Geochem. Geophys. Geosyst. 10 (2).
Konter, J.G., Finlayson, V., Konrad, K., Jackson, M.G., Koppers, A.A., Wessel, P., Bizimis, M., Alverson, A., Kelley, C., 2023. The Longest-lived Pacific Hotspots Reveal a Plume Tail for the Largest Oceanic Plateau. https://doi.org/10.31223/X5CQ2T.
Kopp, H., Kopp, C., Phipps Morgan, J., Flueh, E.R., Weinrebe, W., Morgan, W.J., 2003. Fossil hot spot-ridge interaction in the Musicians Seamount Province: geophysical investigations of hot spot volcanism at volcanic elongated ridges. J. Geophys. Res. Solid Earth 108 (B3).
Koppers, A.A., 2002. ArArCALC—software for 40Ar/39Ar age calculations. Comput. Geosci. 28 (5), 605–619.
Koppers, A.A., Morgan, J.P., Morgan, J.W., Staudigel, H., 2001. Testing the fixed hotspot hypothesis using 40Ar/39Ar age progressions along seamount trails. Earth Planet. Sci. Lett. 185 (3–4), 237–252.
Koppers, A.A., Russell, J.A., Roberts, J., Jackson, M.G., Konter, J.G., Wright, D.J., Staudigel, H., Hart, S.R., 2011. Age systematics of two young en echelon Samoan volcanic trails. Geochem. Geophys. Geosyst. 12 (7).
Kuiper, K.F., Deino, A., Hilgen, F.J., Krijgsman, W., Renne, P.R., Wijbrans, A.J., 2008. Synchronizing rock clocks of Earth history. science 320 (5875), 500–504.
Lee, J.Y., Marti, K., Severinghaus, J.P., Kawamura, K., Yoo, H.S., Lee, J.B., Kim, J.S., 2006. A redetermination of the isotopic abundances of atmospheric Ar. Geochim. Cosmochim. Acta 70 (17), 4507–4512.
Long, X., Geldmacher, J., Hoernle, K., Hauff, F., Wartho, J.A., Garbe-Schönberg, D., Grevemeyer, I., 2019. Age and origin of Researcher Ridge and an explanation for the 14° N anomaly on the Mid-Atlantic Ridge by plume-ridge interaction. Lithos 326, 540–555.
Martin, E., Paquette, J.L., Bosse, V., Ruffet, G., Tiepolo, M., Sigmarsson, O., 2011. Geodynamics of rift–plume interaction in Iceland as constrained by new 40Ar/39Ar and in situ U–Pb zircon ages. Earth Planet. Sci. Lett. 311 (1–2), 28–38.
Matthews, K.J., Seton, M., Müller, R.D., 2012. A global-scale plate reorganization event at 105–100 Ma. Earth Planet. Sci. Lett. 355, 283–298.
Matthews, K.J., Maloney, K.T., Zahirovic, S., Williams, S.E., Seton, M., Müller, R.D., 2016. Global plate boundary evolution and kinematics since the late Paleozoic. Glob. Planet. Chang. 146, 226–250.
Min, K., Mundil, R., Renne, P.R., Ludwig, K.R., 2000. A test for systematic errors in 40Ar/39Ar geochronology through comparison with U/Pb analysis of a 1.1-Ga rhyolite. Geochim. Cosmochim. Acta 64 (1), 73–98.
Mittal, T., Richards, M.A., 2017. Plume-ridge interaction via melt channelization at g alápagos and other near-ridge hotspot provinces. Geochem. Geophys. Geosyst. 18 (4), 1711–1738.
Mixon, E.E., Jicha, B.R., Tootell, D., Singer, B.S., 2022. Optimizing 40Ar/39Ar analyses using an Isotopx NGX-600 mass spectrometer. Chem. Geol. 593, 120753.
Morgan, W.J., 1978. Rodriguez, Darwin, Amsterdam,…, A second type of hotspot island. J. Geophys. Res.: SolidEarth 83 (B11), 5355–5360.
Müller, R.D., Seton, M., Zahirovic, S., Williams, S.E., Matthews, K.J., Wright, N.M., Shephard, G.E., Maloney, K.T., Barnett-Moore, N., Hosseinpour, M., Bower, D.J., 2016. Ocean basin evolution and global-scale plate reorganization events since Pangea breakup. Annu. Rev. Earth Planet. Sci. 44, 107–138.
Müller, R.D., Zahirovic, S., Williams, S.E., Cannon, J., Seton, M., Bower, D.J., Tetley, M. G., Heine, C., Le Breton, E., Liu, S., Russell, S.H., 2019. A global plate model including lithospheric deformation along major rifts and orogens since the Triassic. Tectonics 38 (6), 1884–1907.
Nakanishi, M., Sager, W.W., Klaus, A., 1999. Magnetic lineations within Shatsky rise, Northwest Pacific Ocean: implications for hot spot-triple junction interaction and oceanic plateau formation. J. Geophys. Res. Solid Earth 104 (B4), 7539–7556.
O'Connor, J.M., Hoernle, K., Müller, R.D., Morgan, J.P., Butterworth, N.P., Hauff, F., Sandwell, D.T., Jokat, W., Wijbrans, J.R., Stoffers, P., 2015. Deformation-related volcanism in the Pacific Ocean linked to the Hawaiian–Emperor bend. Nat. Geosci. 8 (5), 393–397.
Ogg, J.G., 2020. Geomagnetic polarity time scale. In: Geologic time scale 2020. Elsevier, pp. 159–192.
Pringle Jr., M.S., 1992. Geochronology and Petrology of the Musicians Seamounts, and the Search for Hot Spot Volcanism in the Cretaceous Pacific (Doctoral Dissertation).
Rea, D.K., 1970. Changes in structure and trend of fracture zones north of the Hawaiian Ridge and relation to sea-floor spreading. J. Geophys. Res. 75 (8), 1421–1430.
Rea, D.K., Naugler, F.P., 1971. Musicians seamount province and related crustal structures north of the Hawaiian ridge. Mar. Geol. 10 (2), 89–111.
Sager, W.W., Pringle, M.S., 1987. Paleomagnetic constraints on the origin and evolution of the Musicians and South Hawaiian seamounts, Central Pacific Ocean. Seamounts, Islands, Atolls 43, 133–162.
Sandwell, D.T., Winterer, E.L., Mammerickx, J., Duncan, R.A., Lynch, M.A., Levitt, D.A., Johnson, C.L., 1995. Evidence for diffuse extension of the Pacific plate from Pukapuka ridges and cross-grain gravity lineations. J. Geophys. Res. Solid Earth 100 (B8), 15087–15099.
Schaen, A.J., Jicha, B.R., Hodges, K.V., Vermeesch, P., Stelten, M.E., Mercer, C.M., Phillips, D., Rivera, T.A., Jourdan, F., Matchan, E.L., Hemming, S.R., 2021. Interpreting and reporting 40Ar/39Ar geochronologic data. Bulletin 133 (3–4), 461–487.
Sotomayor, A., Balbas, A., Konrad, K., Koppers, A.A., Konter, J.G., Wanless, V.D., Hourigan, T.F., Kelley, C., Raineault, N., 2023. New insights into the age and origin of two small cretaceous seamount chains proximal to the Northwestern Hawaiian Ridge. Geosphere 19 (2), 383–405.
Steinberger, B., Gaina, C., 2007. Plate-tectonic reconstructions predict part of the Hawaiian hotspot track to be preserved in the Bering Sea. Geology 35 (5), 407–410.
Tarduno, J.A., Duncan, R.A., Scholl, D.W., Cottrell, R.D., Steinberger, B., Thordarson, T., Kerr, B.C., Neal, C.R., Frey, F.A., Torii, M., Carvallo, C., 2003. The Emperor Seamounts: Southward motion of the Hawaiian hotspot plume in Earth's mantle. Science 301 (5636), 1064–1069.
Tetley, M.G., Williams, S.E., Gurnis, M., Flament, N., Müller, R.D., 2019. Constraining absolute plate motions since the Triassic. J. Geophys. Res. Solid Earth 124 (7), 7231–7258.
Torsvik, T.H., Doubrovine, P.V., Steinberger, B., Gaina, C., Spakman, W., Domeier, M., 2017. Pacific plate motion change caused the Hawaiian-Emperor Bend. Nat. Commun. 8 (1), 15660.
Torsvik, T.H., Steinberger, B., Shephard, G.E., Doubrovine, P.V., Gaina, C., Domeier, M., Conrad, C.P., Sager, W.W., 2019. Pacific-Panthalassic reconstructions: overview, errata and the way forward. Geochem. Geophys. Geosyst. 20 (7), 3659–3689.
Wessel, P., Kroenke, L., 1997. A geometric technique for relocating hotspots and refining absolute plate motions. Nature 387 (6631), 365–369.
Wessel, P., Kroenke, L.W., 2008. Pacific absolute plate motion since 145 Ma: an assessment of the fixed hot spot hypothesis. J. Geophys. Res. Solid Earth 113 (B6).